Phase coexistence in polydisperse mixture of hard-sphere colloidal and flexible chain particles

Yurij V. Kalyuzhnyi[1] and Peter T. Cummings[2]

[1] *Institute for Condensed Matter Physics, Svientsitskoho 1, 79011 Lviv, Ukraine*
[2] *Department of Chemical Engineering, Vanderbilt University, Nashville, TN 37235-1604, USA and Chemical Sciences Division, Oak Ridge National Laboratory, Oak Ridge, TN 27831-6110, USA*

arXiv:0705.1349v1 [cond-mat.soft] 9 May 2007

PACS 64.10.+h – First pacs description
PACS 64.70.Fx – Second pacs description
PACS 82.70.Dd – Third pacs description

Abstract. - A theoretical scheme for the calculation of the full phase diagram (including cloud and shadow curves, binodals and distribution functions of the coexisting phases) for colloid-polymer mixtures with polymer chain length polydispersity and hard-sphere colloidal and polymeric monomer sizes polydispersity is proposed. The scheme combines thermodynamic perturbation theory for associating fluids and recently developed method used to determine the phase diagram of polydisperse spherical shape colloidal fluids (L.Bellier-Castella *et al.*, *J.Chem.Phys.* **113**, 8337(2000)). By way of illustration we present and discuss the full phase diagram for the mixture with polydispersity in the size of the hard-sphere colloidal particles.

Introduction. – Since the pioneering studies of Asakura and Oosawa [1,2] and Vrij [3] substantial amount of efforts have been focused on the development of the theoretical methods describing the phase behavior of the athermal colloid-polymer mixtures (see Refs. [4–6] and references therein). Usually in the vast majority of the theories developed so far interaction between polymers is either ignored or treated using approximations different from those assumed to describe polymer-colloid and colloid-colloid interactions. This feature imposes certain restrictions on the possibilities of the theory, for example the theories, which ignore polymer-polymer interactions are restricted to the mixtures of short polymers and large colloidal particles (ideal polymer limit). Recently an attempt to describe the phase behavior of the colloid-polymer mixture with both components treated on an equal footing using polymer reference interaction site model integral-equation approach [7] and thermodynamic perturbation theory (TPT) for associating fluids [6] was made. In these studies polymer molecules were modeled as a flexible chains of tangentially bonded hard-sphere monomers and colloidal particles were represented as a hard spheres. Later TPT approach was extended [8] to account for the chain length polydispersity effects. In this study we propose further extension of the TPT to account for polydispersity in the polymer chain length and in the hard-sphere sizes of both colloidal particles and polymer monomers. This extension is based on the previously developed method [9, 10], which allows us to determine the full phase diagram (including binodals and cloud and shadow curves) and to discuss fractionation effects on the level of the distribution functions of the two daughter phases.

The model. – We consider polydisperse mixture of hard-sphere flexible chain particles represented by m tangentially bonded hard spheres of diameter σ. In the following we will distinguish between $p-$type of the particles (polymers) and $c-$type of the particles (colloids). Thus the species of each particle is characterized by the set of three variables (a, m, σ) with a denoting the type of the particle (either p or c), $m = 1, 2, ..., \infty$ and $0 \leq \sigma < \infty$. The number density of the $a-$type of the particles is ρ_a and the overall number density ρ is $\rho = \rho_p + \rho_c$. The species variables a, m and σ are distributed according to the distribution function $F_a(m, \sigma)$, which is positive and satisfies the following normalizing conditions

$$\sum_a \sum_m \int d\sigma \; F_a(m, \sigma) = 1. \tag{1}$$

Further we put $F_a(m,\sigma)=\alpha_a f_a(m,\sigma)$, where α_a denote the fraction of the $a-$type of the particles

$$\alpha_a=\sum_m\int d\sigma\ F_a(m,\sigma); \tag{2}$$

obviously, $\alpha_p+\alpha_c=1$ and partial distribution functions $f_a(m,\sigma)$ are normalized.

Thermodynamical properties. – Thermodynamical properties of the model at hand are calculated using TPT of Wertheim [11,12]. According to TPT Helmholtz free energy of the system A is represented as a sum of three terms $A=A_{id}+A_{hs}+A_{ch}$, where A_{id} is the ideal gas term

$$\frac{A_{id}}{VkT}=\sum_a\rho_a\sum_m\int d\sigma\ F_a(m,\sigma)\left\{\ln\left[\rho_a F_a(m,\sigma)\right]-1\right\}, \tag{3}$$

A_{hs} is the hard-sphere term

$$\frac{A_{hs}}{VkT}=\frac{6}{\pi}\left[\left(\frac{\zeta_2^3}{\zeta_3^2}-\zeta_0\right)\ln\Delta+\frac{3\zeta_1\zeta_2}{\Delta}+\frac{\zeta_2^3}{\zeta_3\Delta^2}\right], \tag{4}$$

and A_{ch} is the term describing formation of the chains

$$\frac{A_{ch}}{VkT}=\sum_a\rho_a\sum_m(1-m)\int d\sigma\ F_a(m,\sigma)\ln g_{aa}^{(hs)}(\sigma). \tag{5}$$

Here V is the system volume, k is the Boltzmann constant, T is the temperature, $\zeta_0,\zeta_1,\zeta_2,\zeta_3$ are the distribution function moments

$$\zeta_n=\frac{\pi}{6}\rho\sum_a\sum_m m\int d\sigma\ F_a(m,\sigma)\sigma^n,\qquad n=0,1,2,3; \tag{6}$$

$\Delta=1-\zeta_3$, $g_{aa}^{(hs)}(\sigma)$ is the hard-sphere contact value

$$g_{aa}^{(hs)}(\sigma)=\frac{1}{\Delta}\left(1+\frac{3}{2}\sigma\frac{\zeta_2}{\Delta}+\frac{1}{2}\sigma^2\frac{\zeta_2^2}{\Delta^2}\right). \tag{7}$$

In (4) and (7) Boublik's [13] and Mansoori's *et al.* [14] expressions for A_{hs} and $g_{aa}^{(hs)}(\sigma)$ have been utilized. All the rest of thermodynamical properties can be obtained from Helmholtz free energy using the standard thermodynamical relations. Taking the volume derivative of the free energy we get the following expression for the pressure: $\beta P=\rho+\beta P_{hs}+\beta P_{ch}$, where

$$\beta P_{hs}=\frac{6}{\pi\Delta}\left\{\zeta_0\zeta_3+\frac{\zeta_2}{\Delta}\left[3\zeta_1+\frac{\zeta_2^2}{\Delta}(2+\Delta)\right]\right\}, \tag{8}$$

$$\beta P_{ch}=\frac{1}{\Delta}\left(\zeta_3\Omega+\zeta_2\Psi\right), \tag{9}$$

$$\Omega=\rho\sum_a\sum_m(1-m)\int d\sigma\ F_a(m,\sigma)\Omega(\sigma), \tag{10}$$

$$\Psi=\rho\sum_a\sum_m(1-m)\int d\sigma\ F_a(m,\sigma)\Psi(\sigma), \tag{11}$$

$$\Omega(\sigma)=\frac{\Delta^2+3\sigma\zeta_2\left(\Delta+\frac{1}{2}\sigma\zeta_2\right)}{\Delta^2+\frac{3}{2}\sigma\zeta_2\left(\Delta+\frac{1}{3}\sigma\zeta_2\right)}, \tag{12}$$

$$\Psi(\sigma)=\frac{\frac{3}{2}\sigma\Delta\left(\Delta+\frac{2}{3}\sigma\zeta_2\right)}{\Delta^2+\frac{3}{2}\sigma\zeta_2\left(\Delta+\frac{1}{3}\sigma\zeta_2\right)}. \tag{13}$$

Chemical potential is obtained as the functional derivative of the free energy density F/V with respect to the function $\rho_a(m,\sigma)=\rho_a F_a(m,\sigma)$:

$$\mu_a(m,\sigma)=\ln\left[\rho_a F(m,\sigma)\right]+\mu_{a,hs}(m,\sigma)+\mu_{a,ch}(m,\sigma), \tag{14}$$

where

$$\beta\mu_{a,hs}(m,\sigma)=m\left[\sigma^2\frac{\zeta_2^2}{\zeta_3^2}\left(3-2\sigma\frac{\zeta_2}{\zeta_3}\right)-1\right]\ln\Delta$$
$$+\frac{\pi m}{2\Delta}\sigma\left\{\sigma^2\left[\frac{2}{\pi}\zeta_0-\frac{\zeta_2^3}{\zeta_3^2}\frac{(1+\Delta)}{3\Delta}+\frac{\pi}{3\Delta}\zeta_2\left(\frac{1}{2}\zeta_1+\frac{1}{3}\frac{\zeta_2^2}{\zeta_3\Delta}\right)\right]\right.$$
$$\left.+\zeta_2\left(1+\sigma\frac{\zeta_2}{\zeta_3\Delta}\right)+\sigma\zeta_1\right\}, \tag{15}$$

$$\beta\mu_{a,ch}(m,\sigma)=(1-m)\ln g_{aa}(\sigma)+\frac{\pi}{6}\frac{m\sigma^2}{\Delta}\left(\Omega\sigma+\Psi\right). \tag{16}$$

One can easily see that thermodynamical properties of the model at hand are defined by the set of a finite number of the distribution function moments, i.e. four regular moments $\zeta_0,\zeta_1,\zeta_2,\zeta_3$ and two generalized moments (Ω, Ψ). Thus polydisperse mixture of the chain particles treated within TPT belong to the class of truncatable free energy models [15].

Phase equilibrium conditions. – We assume that at a certain density $\rho^{(0)}$ and composition $F_a^{(0)}(m,\sigma)$ the system separates into two phases with the densities $\rho^{(1)}$ and $\rho^{(2)}$, and compositions $F_a^{(1)}(m,\sigma)$ and $F_a^{(2)}(m,\sigma)$. Hereafter the upper index (0) refer to the parent phase and the upper indices (1) and (2) refer to the daughter phases. At equilibrium these quantities take the values, which follows from the phase equilibrium conditions, i.e.: (i) conservation of the total volume of the system, (ii) conservation of the total number of the particles of each species, (iii) equality of the chemical potentials of particles of the same species in the coexisting phases, (iv) equality of the pressure in the coexisting phases. These conditions finally lead to the following set of relations [9,10]:

$$F_a^{(\alpha)}(m,\sigma)=F_a^{(0)}(m,\sigma)$$
$$\times Q_a^{(\alpha)}\left(m,\sigma;\rho^{(0)},\rho^{(1)},\rho^{(2)};\left[F_p^{(\alpha)},F_c^{(\alpha)}\right]\right), \tag{17}$$

$$P^{(1)}\left(\rho^{(1)};\left[F_p^{(1)},F_c^{(1)}\right]\right)=P^{(2)}\left(\rho^{(2)};\left[F_p^{(2)},F_c^{(2)}\right]\right), \tag{18}$$

$$\sum_a\sum_m\int d\sigma\ F_a^{(\alpha)}(m,\sigma)=1,\quad\text{for }\alpha=1\text{ or }\alpha=2, \tag{19}$$

where

$$\rho^{(\alpha)}Q_a^{(\alpha)}\left(m,\sigma;\rho^{(0)},\rho^{(1)},\rho^{(2)};\left[F_p^{(\alpha)},F_c^{(\alpha)}\right]\right)$$

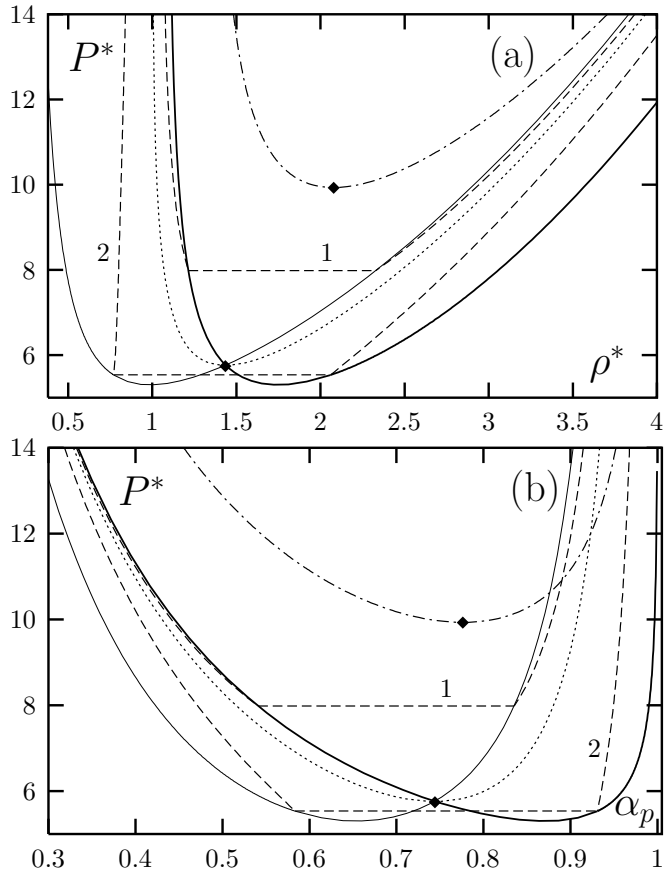

Fig. 1: Phase diagram in: (a) P^* vs ρ^* and (b) P^* vs α_p coordinate frames. Cloud and shadow curves are represented by thick and thin solid lines, respectively, binodal curves with: (1) $\alpha_p^{(0)} = 0.541$ and (2) $\alpha_p^{(0)} = 0.931$ by the broken lines and with $\alpha_p^{(0)} = \alpha_{p,cr}^{(0)} = 0.744$ by the dotted line. The dashed-dotted line denotes the binodal curve for the bidisperse version of the model and critical points are indicated by the diamonds.

$$= \frac{\rho^{(0)}\left(\rho^{(2)}-\rho^{(1)}\right)\left[1-\delta_{1\alpha}+\delta_{1\alpha}\exp\left(\beta\Delta\tilde{\mu}_a\right)\right]}{\rho^{(0)}-\rho^{(1)}-\left(\rho^{(0)}-\rho^{(2)}\right)\exp\left(\beta\Delta\tilde{\mu}_a\right)}, \quad (20)$$

$$\Delta\tilde{\mu}_a = \tilde{\mu}_a^{(2)}\left(m,\sigma,\rho^{(2)};\left[F_a^{(2)}\right]\right) - \tilde{\mu}_a^{(1)}\left(m,\sigma,\rho^{(1)};\left[F_a^{(1)}\right]\right), \quad (21)$$

$\tilde{\mu}_a^{(\alpha)}$ is the excess (over the ideal gas) chemical potential of the particle (a,m,σ) in the phase α and $[\ldots]$ denote functional dependence. The relation between $F_a^{(0)}(m,\sigma)$ and daughter phase distribution function $F_a^{(\alpha)}(m,\sigma)$, i.e., Eq. (17), follows from the phase equilibrium conditions (i)-(iii).

Relations (17)-(19) represent a closed set of equations to be solved for the unknowns $\rho^{(\alpha)}$ and $F_a^{(\alpha)}(m,\sigma)$; this set have to be solved for every value of the species variables a, m and σ. However, since thermodynamical properties of the model at hand are defined by the finite number of the moments we can map this set of equations onto a closed set of fourteen algebraic equations for $\rho^{(\alpha)}$ and twelve moments $\zeta_n^{(\alpha)}$ $(n=0,1,2,3)$, $\Omega^{(\alpha)}$ and $\Psi^{(\alpha)}$, where $\alpha = 1,2$. We have

$$\zeta_n^{(\alpha)} = \rho^{(\alpha)}\sum_a\sum_m m\int d\sigma\ \sigma^n F_a^{(0)}(m,\sigma) \times Q_a^{(\alpha)}\left(m,\sigma,\rho^{(0)};\left\{X^{(1)}\right\},\left\{X^{(2)}\right\}\right), \quad (22)$$

$$\Omega^{(\alpha)} = \rho^{(\alpha)}\sum_a\sum_m (1-m)\int d\sigma\ \Omega(\sigma) F_a^{(0)}(m,\sigma) \times Q_a^{(\alpha)}\left(m,\sigma,\rho^{(0)};\left\{X^{(1)}\right\},\left\{X^{(2)}\right\}\right), \quad (23)$$

$$\Psi^{(\alpha)} = \rho^{(\alpha)}\sum_a\sum_m (1-m)\int d\sigma\ \Psi(\sigma) F_a^{(0)}(m,\sigma) \times Q_a^{(\alpha)}\left(m,\sigma,\rho^{(0)};\left\{X^{(1)}\right\},\left\{X^{(2)}\right\}\right), \quad (24)$$

where $\left\{X^{(\alpha)}\right\}$ represent unknowns of the problem, i.e.

$$\left\{X^{(\alpha)}\right\} = \left\{\rho^{(\alpha)},\zeta_n^{\alpha},\Omega^{(\alpha)},\Psi^{(\alpha)}\right\},\ n=0,1,2,3;\ \alpha=1,2.$$

The remaining two equations follows from the equality of the pressure in coexisting phases (18),

$$P^{(1)}\left(\rho^{(1)};\left\{X^{(1)}\right\}\right) = P^{(2)}\left(\rho^{(2)};\left\{X^{(2)}\right\}\right), \quad (25)$$

and from the normalizing condition (19) for either phase $\alpha = 1$ or $\alpha = 2$,

$$\sum_a\sum_m\int d\sigma\ F_a^{(0)}(m,\sigma) \times Q_a^{(\alpha)}\left(m,\sigma,\rho^{(0)};\left\{X^{(1)}\right\},\left\{X^{(2)}\right\}\right) = 1. \quad (26)$$

Solution of the set of equations (22)-(26) for a given density $\rho^{(0)}$ and distribution function $F_a^{(0)}(m,\sigma)$ of the parent phase gives the densities $\rho^{(\alpha)}$ and distribution functions $F_a^{(\alpha)}(m,\sigma)$ of the two coexisting daughter phases. The coexisting densities at different densities of the parent phase $\rho^{(0)}$ defined binodals, which are terminated when a density of one of the phases is equal to the parent phase density $\rho^{(0)}$. For the different values of the colloidal (and polymer) particles fraction $\alpha_c^{(0)}$ ($\alpha_p^{(0)} = 1-\alpha_c^{(0)}$) in the parent phase these termination points form the cloud and shadow coexisting curves. These curves intersect at the critical point, which is characterized by the critical density $\rho_{cr} = \rho^{(1)} = \rho^{(2)} = \rho^{(0)}$ and critical colloidal (and polymeric) composition $\alpha_{c,cr} = \alpha_c^{(1)} = \alpha_c^{(2)} = \alpha_c^{(0)}$ ($\alpha_{p,cr} = 1-\alpha_{c,cr}$). The cloud-shadow curves can be obtained as a special solution of the general coexisting problem, when the properties of one phase are equal to the properties of the parent phase: assuming that the phase $\alpha = 2$ is the cloud phase, i.e. $\rho^{(2)} = \rho^{(0)}$, and following the above scheme we will end up with the same set of equations (22)-(26), but with $\rho^{(2)}$ and $F_a^{(2)}(m,\sigma)$ substituted by $\rho^{(0)}$ and $F_a^{(0)}(m,\sigma)$, respectively.

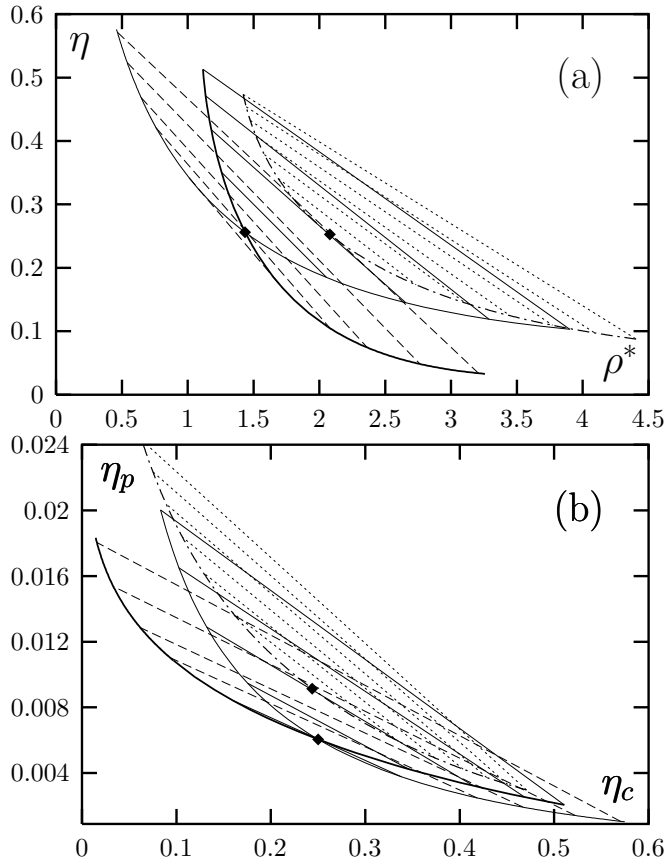

Fig. 2: The same as in Figure 1 in: (a) η vs ρ^* and (b) η_p vs η_c coordinate frames. Thin solid tie lines and broken tie lines connect the points on the cloud and shadow curves and dotted tie lines connect the points on the binodal curve for the bidisperse version of the model.

Results and discussion. – To illustrate the scheme developed in the previous sections we present here numerical results for the phase behavior of the polydisperse mixture of colloidal and polymeric particles with poydispersity in the size of the colloidal particles only. Colloids are represented by the polydisperse mixture of hard spheres and polymers are modeled by the hard-sphere flexible chains with fixed chain length m_0 and hard-sphere size of the monomeric units σ_p. Thus for the distribution function of the parent phase $F_a^{(0)}(m,\sigma)$ we have

$$F_p^{(0)}(m,\sigma) = \alpha_p^{(0)} \delta\left(\sigma - \sigma_p\right) \delta_{m,m_0}, \tag{27}$$

$$F_c^{(0)}(m,\sigma) = \alpha_c^{(0)} f_c^{(0)}(\sigma) \delta_{m,1}, \tag{28}$$

where for the colloidal diameter distribution $f_c^{(0)}(\sigma)$ we have chosen beta-distribution, given by

$$f_c^{(0)}(\sigma) = B^{-1}(\gamma,\nu) \left(\frac{\sigma}{\sigma_m}\right)^{\gamma-1} \left(1 - \frac{\sigma}{\sigma_m}\right)^{\nu-1} \theta\left(\sigma_m - \sigma\right),$$

where $\theta(x)$ is the Heaviside step function, $B(\gamma,\nu)$ is the Beta function [10] and γ and ν are related to the first

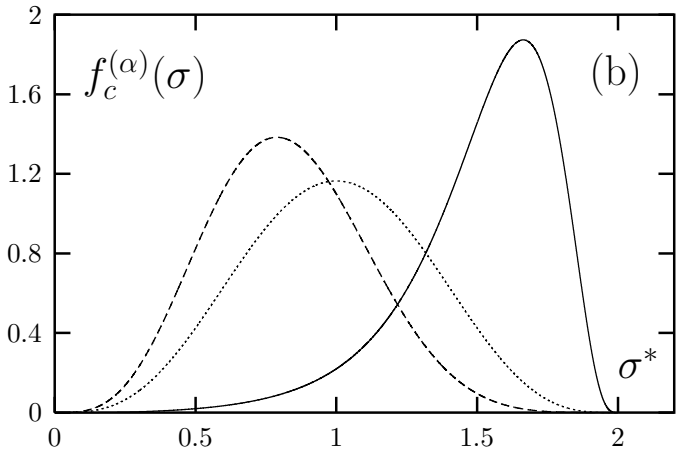

Fig. 3: Distribution functions of the parent phase (dotted line), low density phase (solid line) and high density phase (dashed line) on the shadow curve at $P^* = 8$. Here $\sigma^* = \sigma/\langle\sigma\rangle_c^{(0)}$

$\langle\sigma\rangle_c^{(0)}$ and second $\langle\sigma^2\rangle_c^{(0)}$ moments by

$$\gamma = \frac{\sigma_m - \langle\sigma\rangle_c^{(0)}\left(1 + D_\sigma^{(0)}\right)}{D_\sigma^{(0)}\sigma_m}, \quad \nu = \left(\frac{\sigma_m - \langle\sigma\rangle_c^{(0)}}{\langle\sigma\rangle_c^{(0)}}\right)\gamma$$

with

$$\langle\sigma^n\rangle_c^{(\alpha)} = \int d\sigma\ \sigma^n f_c^{(\alpha)}(\sigma),\ D_\sigma^{(\alpha)} = \langle\sigma^2\rangle_c^{(\alpha)} / \left(\langle\sigma\rangle_c^{(\alpha)}\right)^2 - 1. \tag{29}$$

Calculations were carried out for the model parameters chosen to be: $m_0 = 50$, $\sigma_p/\langle\sigma\rangle_c^{(0)} = 0.06$, $D_\sigma = 0.1$ and $\sigma_m/\langle\sigma\rangle_c^{(0)} = 2$.

At sufficiently low density of the parent phase $\rho^{(0)}$ the mixture is stable as a single phase. As $\rho^{(0)}$ is increased the system will phase separate into two phases: low density phase and high density phase. In Figures 1 and 2 we show the phase diagram in a different coordinate frames, i.e. P^* vs ρ^* (Fig. 1a), P^* vs α_p (Fig. 1b), η vs ρ^* (Fig. 2a) and η_p vs η_c (Fig. 2b) , where $P^* = \beta P(\langle\sigma\rangle_c^{(0)})^3$, $\rho^* = \rho(\langle\sigma\rangle_c^{(0)})^3$, η and η_a are the overall packing fraction and packing fraction of the $a-$type of the particles, respectively. The phase diagram shown in Figure 1 includes the cloud and shadow curves, along with three binodals for three selected parent phase fractions $\alpha_p^{(0)} = 0.541,\ 0.744,\ 0.931$, one of them being the critical fraction $\alpha_{p,cr}^{(0)} = 0.744$. The two branches of the binodals for the two selected $\alpha_p^{(0)}$ values ($\alpha_p^{(0)} = 0.541,\ 0.931$) terminate on the cloud and shadow curve, where the ρ values of the end points of the respective binodals on the cloud curve are equal to the $\rho^{(0)}$ values of the binodals in these points. For the critical value of the parent phase fraction $\alpha_{p,cr}^{(0)} = 0.744$ corresponding binodals meet in the critical point. In Figure 2 we include only the cloud and shadow curves. For the reference in both figures we also display the binodal curve for the bidisperse version of the model ($D_\sigma^{(0)} = 0$). Comparison between

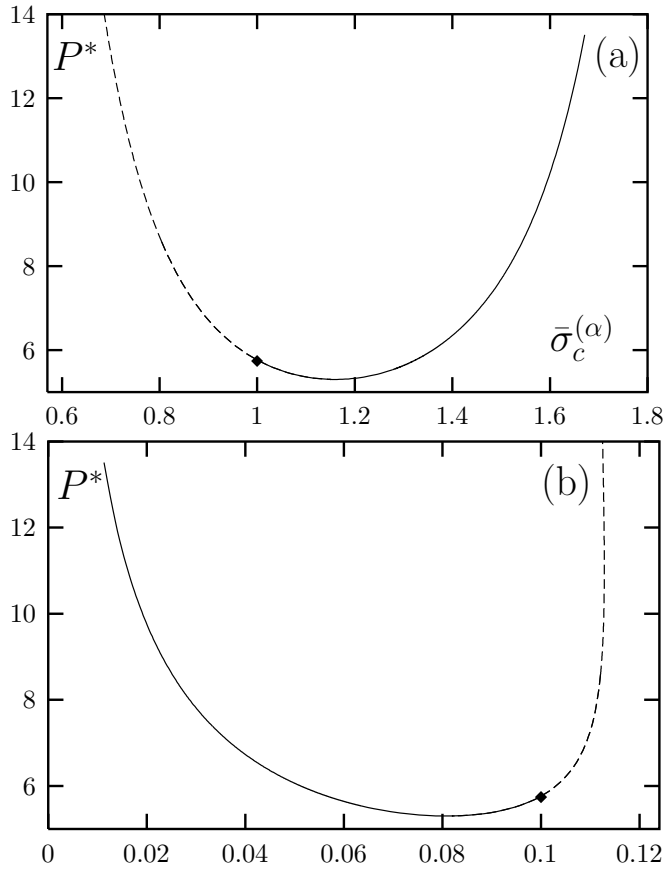

Fig. 4: Average hard-sphere size $\tilde{\sigma}_c^{(\alpha)} = \langle\sigma\rangle_c^{(\alpha)}/\langle\sigma\rangle_c^{(0)}$ (a) and distribution function width $D_\sigma^{(\alpha)}$ (b) of the colloidal particles along the shadow curve. Solid lines represent low density phase and dashed lines denote high density phase. Critical points are indicated by the diamonds.

the bidisperse and polydisperse versions of the colloid-polymer mixture shows that polydispersity extends the region of the phase instability, shifting the critical point to the lower values of the pressure and density ($P^*_{cr,bid} = 9.93$, $P^*_{cr,polyd} = 5.74$, $\rho^*_{cr,bid} = 2.08$, $\rho^*_{cr,polyd} = 1.43$, Fig. 1) and to slightly lower values of the polymer fraction ($\alpha^{(bid)}_{p,cr} = 0.776$, $\alpha^{(polyd)}_{p,cr} = 0.744$, Fig. 1b) and polymer packing fraction ($\eta^{(bid)}_{p,cr} = 0.009$, $\eta^{(polyd)}_{p,cr} = 0.006$, Fig. 2b). Corresponding relative changes of the colloidal ($\eta_{c,cr}$) and overall (η_{cr}) critical packing fraction are negligible.

According to Figure 2 packing fraction of the low density phase is higher than that of the high density phase; thus the density of the liquid-like phase is lower than that of the gas-like phase. This is not surprising as the fraction of the colloidal particles in the low density phase is larger than in the high density phase. In Figure 3 we show daughter phase distribution functions $f_c^{(\alpha)}(\sigma)$ on the shadow curve at $P^* = 8$ together with the parent phase distribution function $f_c^{(0)}(\sigma)$. More detailed information about the composition of the coexisting phases can be extracted from the analysis of the distribution functions of the two daughter phases in terms of their first two moments, $\langle\sigma\rangle_c^{(\alpha)}$ and $D_\sigma^{(\alpha)}$ (29). These two quantities characterize size-distribution of the particles and distribution function width, respectively. In Figure 4 we present $\langle\sigma\rangle_c^{(\alpha)}$ and $D_\sigma^{(\alpha)}$ along the shadow curve. It can be seen that the larger size particles prefer the lower density phase and the smaller size particles are predominantly encountered in the higher density phase. As the pressure increases we observe increase in the mean size of the particles and decrease in the distribution function width in the low-density phase and decrease in the mean size of the particles and increase in the distribution function width in the high-density phase. The magnitude of these changes for the mean size of the particles in both phases are similar (Fig 4a): we observe a strong sharpening of the low-density phase distribution function with increasing pressure, while increase in the width of the high-density phase distribution function do not exceed 13% of its parent phase value (Fig. 4b). A more detailed and systematic investigation of these effects for the mixture with polydispersity in both colloidal and polymeric subsystems will be postponed to a future contributions.

Conclusions. – With the concept presented above we are able to calculate the full phase diagram of polydisperse hard-sphere colloidal and flexible chain particles with all types of polydispersity. For a particular system with polydispersity in the size of the colloidal particles we present and discuss the phase diagram and corresponding fractionation effects.

* * *

One of the authors (YVK) was partially supported by the Science & Technology Center in Ukraine (project No. 4140). YVK gratefully acknowledges the hospitality at the Vanderbilt University where part of this work was performed.

REFERENCES

[1] Asakura S. and Oosawa F., *J. Chem. Phys.*, **22** (1954) 1255;
[2] Asakura S. and Oosawa F., *J. Polym. Sci.*, **33** (1958) 183;
[3] Vrij A., *Pure Appl. Chem.*, **48** (1976) 471;
[4] Tuinier R. and Rieger J. and de Kruif C.G., *Adv. Colloid. Interface Sci.*, **103** (2003) 1;
[5] Fuchs M. and Schweizer K.S., *J. Phys. (Condens. Matt.)*, **14** (2002) R239;
[6] Paricaud P. and Varga S. and Jackson G., *J. Chem. Phys.*, **118** (2003) 8525;
[7] Ramakrishnan S. and Fuchs M. and Schweizer K.S. and Zukoski C.F., *J. Chem. Phys.*, **116** (2002) 2201;
[8] Paricaud P. and Varga S. and Cummings P.T. and Jackson G., *Chem. Phys. Lett.*, **398** (2004) 489;
[9] Bellier-Castella L. and Xu H. and Baus M., *J. Chem. Phys.*, **113** (2000) 8337;

[10] Kalyuzhnyi Yu.V. and Kahl G., *J. Chem. Phys.*, **119** (2003) 7335;
[11] Wertheim M.S., *J. Chem. Phys.*, **87** (1987) 7323
[12] Chapman W.G. and Jackson G. and Gubbins K.E., *Mol. Phys.*, **65** (1988) 1057;
[13] Boublik T., *J. Chem. Phys.*, **53** (1970) 471;
[14] Mansoori G.A. and Carnahan N.F. and Starling K.E. and Leland I.W., *J. Chem. Phys.*, **54** (1971) 1523;
[15] Sollich P., *J. Phys. (Condens. Matt.)*, **14** (2002) R79;